Meteorol. Appl. 7, 45–60 (2000)

Numerical simulation of monsoon depressions over India with a high-resolution nested regional model

K V J Potty*, U C Mohanty, *Centre for Atmospheric Sciences, Indian Institute of Technology, New Delhi-110 016, India*

S Raman, *Department of Marine, Earth and Atmospheric Sciences, North Carolina State University, Raleigh, NC 27609-8208, USA*

*Present affiliation: *IBM Solutions Research Centre, Indian Institute of Technology, New Delhi-110 016, India*

The structure and track of monsoon depressions over India during the summer monsoon have been simulated using a double-nested limited-area numerical weather prediction model. Four distinct cases of monsoon depressions that formed over the Bay of Bengal and adjoining areas have been studied. Initial conditions for the simulations are from either the European Centre for Medium Range Weather Forecasts, Reading, UK or the National Centre for Medium Range Weather Forecasting, New Delhi, India. The model is integrated for up to 48 hours for each case and the results are compared with verification fields. Forecasts of mean sea level pressure and low-level wind indicate that the location of the centres of the depressions and their track could be predicted satisfactorily even though the magnitude of the central pressure is slightly too high. Temperature forecasts show close agreement with the verification analyses and the distribution of precipitation is well simulated. The vertical cross-sections of temperature and wind forecasts show the correct vertical structure. RMS errors of the mean sea level pressure, wind and temperature indicate that the model could simulate the large-scale fields reasonably well. RMS errors of the tracks of the depressions confirm the fact that the high-resolution nested grid model can predict the tracks of the depressions with reasonable accuracy.

1. Introduction

During the summer monsoon season over India (June–September), a series of low-pressure systems form over the Head Bay of Bengal and move in a west to north-west direction across the northern Indian land mass. Generally, these low-pressure systems have three closed isobars at 2 hPa intervals on a mean sea level pressure chart and they cover 4–5° latitude/longitude square; they are known as monsoon depressions. These systems have surface winds up to 16 m s^{-1} and they produce widespread rain, with the heaviest over the south-west quadrant (Rao, 1976). Some of the depressions fill up before reaching north-west India, while others move along the monsoon trough and finally merge with the seasonal low-pressure area over north-west India. A few of them may recurve northwards and move to the foothills of the Himalayas. With the formation of depressions over the Head Bay of Bengal, the monsoon becomes active over many parts of the country. The monsoon trough, which runs from Pakistan to the Head Bay of Bengal, oscillates to the north and south about its mean position. On some occasions, during the northward movement of a monsoon depression, the monsoon trough swings northwards to the foothills of the Himalayas (Asnani, 1993), and this results in a considerable decrease in rainfall over most parts of the country. This situation is often known as the break monsoon condition. However, during the formation and movement of a monsoon depression, the monsoon trough remains either in its normal position or shifts slightly southwards (Mooley & Shukla, 1987).

A monsoon depression is an extreme weather phenomenon found in the lower troposphere during the summer monsoon season. A large number of observational and diagnostic studies pertaining to monsoon depressions have been made (Das, 1952; Pisharoty & Asnani, 1957; Koteswaram & George, 1958; Rao & Rajamani, 1970; Srinivasan *et al.*, 1971; Godbole, 1977; Sikka, 1977; Warner, 1984 and many others). Godbole (1977) has constructed a composite structure of the monsoon depression based on five cases. The study showed that the strongest activity is concentrated in a narrow zone ahead of the depression where there is strong cyclonic vorticity, convergence and ascent. Relatively weak activity is found behind the depression. He also found

that the strongest winds occur in the south-west quadrant of the depression. The thermal structure of the monsoon depression is such that there is a cold core in the lower tropospheric levels and a warm core above, and it has a horizontal dimension of about 500 km with a vertical extent up to about 8 km (~400 hPa). Observational studies show a strong vertical tilt of the depression towards colder air aloft, suggesting the importance of vertical shear in the formation of monsoon depressions. Theoretical studies also show the importance of vertical shear and CISK in the growth of depressions. Warner (1984) has provided a detailed observational analysis of the convective elements as seen from satellite imagery and aircraft photogrammetry.

Modelling studies on individual monsoon depressions have also been carried out by different researchers. The dynamics, energetics and numerical weather prediction aspects of a monsoon depression were investigated with a hierarchy of numerical models by Krishnamurti *et al.* (1976). The study focussed on the evolutionary aspect of the depression but did not cover its formative stage. Krishnamurti *et al.* (1977) first pointed out that some monsoon depressions do not seem to form in situ over the Bay of Bengal. Krishnamurti (1977) simulated the track of a depression and found that the meridional slope of the mountains had a strong influence on the motion of the depression. Krishnamurti *et al.* (1983, 1984) also carried out detailed research on the prediction of monsoon depressions using a global spectral model and a subsequent diagnosis of the simulated results by making use of initial conditions from the FGGE/MONEX observations. Lindzen *et al.* (1983) ascribed the growth of a monsoon depression to the horizontal shear flow instability mechanism. Pearce (1981) used a linear quasi-geostrophic model to investigate the phenomenon of downstream development of monsoon depressions. He found that the main downstream effect is the generation of westward-moving upper-level baroclinic disturbances. Shukla (1977) carried out a linear instability analysis of an observed mean zonal flow in the cross-section along 85° E for a quantitative explanation for the genesis of monsoon depressions.

Because of the important role played by monsoon depressions in the distribution of rainfall over the country, it is of interest to study the predictability of the tracks of these monsoon depressions and their structure. In this study an attempt is made to simulate the precipitation, wind, temperature field etc. associated with monsoon depressions using a high-resolution nested grid limited-area model (LAM). The tracks of a number of monsoon depressions are also considered. The overall performance of a LAM in simulating important characteristic features of monsoon depressions is examined.

2. Model description and experimental design

A nested grid model with a terrain following coordinate is used in this study. The model has two parts: a fine-resolution grid part (hereafter referred as FRG) and a coarse-resolution grid part (hereafter referred as CRG). The model has been nested in such a way that every third point of the FRG is collocated with the CRG grid points and the flow of information is only from CRG to FRG. The lateral boundary conditions provided for the models are based on the scheme by

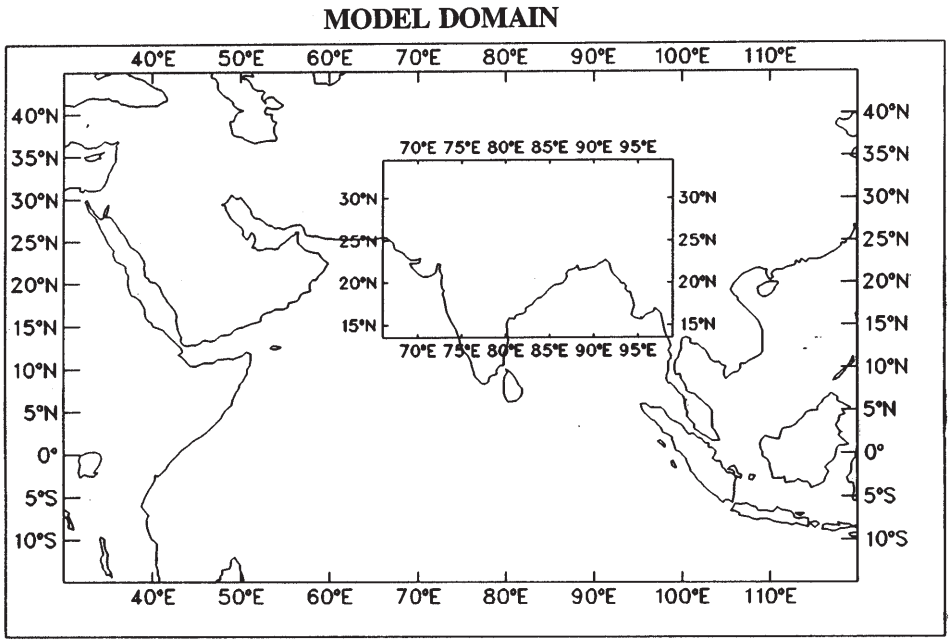

Figure 1. *Model domain chosen for the outer coarse resolution (30°–120° E, 15° S – 45° N; horizontal resolution 1.5° lat./long.) and the inner fine resolution (66°–99° E, 13.5°–34.5° N; horizontal resolution 0.5° lat./long.) model parts.*

Table 1. *Initial conditions chosen for integrating the model and their sources.*

Case study	Initial conditions	Sources of analysed data sets
Case I	3 August 1988, 1200 UTC	ECMWF, UK
Case II	5 August 1988, 1200 UTC	ECMWF, UK
Case III	17 August 1994, 0000 UTC	NCMRWF, India
Case IV	2 September 1995, 0000 UTC	NCMRWF, India

Davies (1976, 1983). For the FRG domain, the sponge boundary condition of Perkey & Kreitzberg (1976) is employed for updating the lateral boundaries of the model. Both the model parts have 16 levels in the vertical with 8 levels in the planetary boundary layer (PBL). The physical processes included in this primitive equation model are associated with dry convective adjustment, large-scale precipitation, convective precipitation and the PBL. More details of the model are given in the Appendix.

The domain of CRG covers most of the Indian summer monsoon circulation region, which includes the Bay of Bengal and the Arabian Sea. Within this domain lies the FRG, which covers almost the entire monsoon trough region and the areas of formation and movement of monsoon depressions (Figure 1). The horizontal resolution of the CRG is 1.5° latitude/longitude and that of FRG is 0.5° latitude/longitude.

Four cases of monsoon depressions are selected for the study. Out of the four cases chosen, initial conditions for two cases are obtained from the operational analyses of the European Centre for Medium Range Weather Forecasts (ECMWF), Reading, UK and for the other two cases they come from analyses produced by the National Centre for Medium Range Weather Forecasting (NCMRWF), New Delhi, India. Initial conditions used for the numerical simulations are summarized in Table 1. The horizontal resolution of the initial conditions taken from ECMWF was 1.875° latitude/longitude whereas that obtained from NCMRWF was 1.5° latitude/longitude.

3. Synoptic conditions

The monsoon was active during the whole month of August 1988 throughout India. During the month, the seasonal monsoon trough in the lower levels was well organized. The depression which developed over the North Bay of Bengal on 2 August 1988 had a long track in a north-westerly direction across the northern part of India (see Figure 2). The analyses for this period are taken as the initial conditions for Cases I and II (1200 UTC on 3 and 5 August 1988 respectively). The central pressure of the depression on 2 August 1988 was 994.5 hPa. It then moved over the central part of India and further intensified. The central pressure on 4 August was 993.5 hPa. The system intensified further and on the 5th the central pressure became 992 hPa. The depression started dissipating on the 6th and it merged with the seasonal low over southern Pakistan on the 7th. The observed mean sea level pressures from 2 to 7 August 1988 at 0300 UTC are given in Figure 2. During the long passage across the country, copious rainfall occurred along the track of the depression.

A monsoon depression that formed over the north-west Bay of Bengal at 0000 UTC on 17 August 1994 (Figure 3(*a*)) has been chosen as the initial condition for Case III. The central pressure of the depression was 995 hPa on 17 August 1994. The system further deepened and intensified on the 18th and moved inland in a west–north-westerly direction. The position of the depression at 0000 UTC on the 18th and 19th is also given, in Figures 3(*b*) and 3(*c*) respectively. On 19 August at 0000 UTC, the depression was located over central India. It weakened into a low-pressure area over south-west Pakistan on the morning of the 21st. Under its influence, the south-west monsoon strengthened over the central parts of the country. During its passage, large rainfall rates were reported along its track.

On 1 September 1995 at 0000 UTC, landfall occurred for a low pressure system which formed over the central Bay of Bengal (Case IV). On the 2nd, it intensified into a depression and reached a pressure of 992 hPa as it moved in a north–north-westerly direction. On the 3rd, it further deepened to 991 hPa, and on the 4th it arrived over the northern part of India. From the 5th onwards it started dissipating and finally merged with the seasonal low on 6 September 1995. During its passage, it produced copious rainfall over the region. The observed mean sea level pressure for these days is illustrated in Figure 4.

Since the objective of this paper is to simulate the structure and track of monsoon depressions and to study the meteorological activities in and around the depression zone and along its track, only the simulation from the fine resolution grid (FRG) part of the nested model is presented here.

4. Surface pressure forecasts

The 24-hour forecast of mean sea level pressure by the model for all four cases and the corresponding verification analyses are depicted in Figure 5. The results show that the locations of the centres of the depressions and their tracks were predicted reasonably well for all cases,

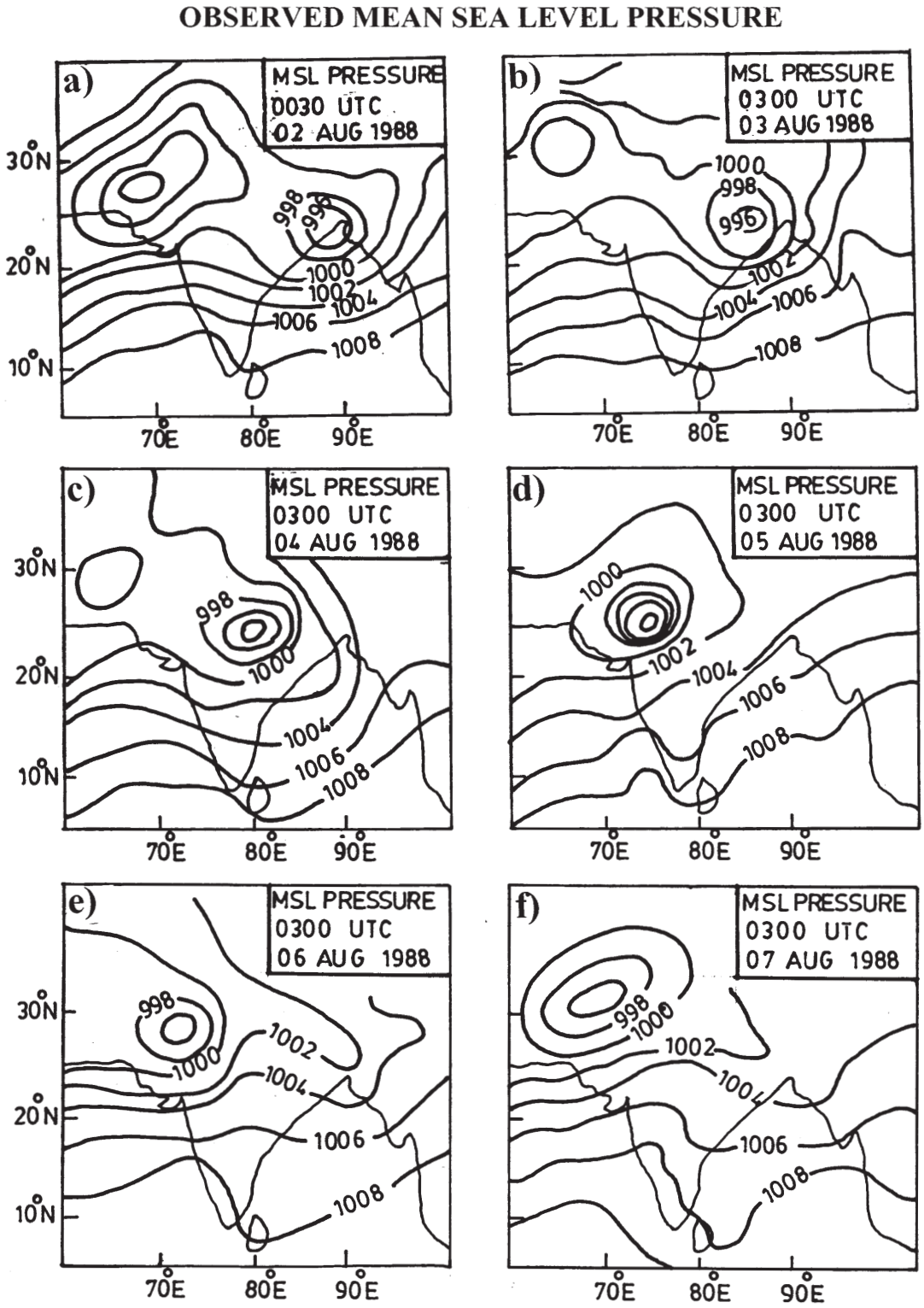

Figure 2. *Observed mean sea level pressure (contour interval: 2 hPa) at 0300 UTC at on (a) 2 August 1988, (b) 3 August 1988, (c) 4 August 1988, (d) 5 August 1988, (e) 6 August 1988 and (f) 7 August 1988. (Source: India Met. Dept.)*

but the magnitude of the central pressure is found to be somewhat higher than that analysed. For Case I, the central pressure of the system given by the verification analysis is 993.2 hPa (Figure 5(*a*)) and that simulated is 993.6 hPa (Figure 5(*b*)). Table 2 gives the comparison of central pressure and their location between the forecast (both at 24 and 48 hours) and the corresponding verification analyses for all the four cases. The location of the centre of the depression of Case I shows a more organised and intense circulation to the south of the verifying analysis. Further, the model simulated an elongated closed isobar of 998 hPa along the monsoon trough region similar to the analysis. Over the oceanic region and over the peninsular regions, the model predicted the pressure distribution very close to the analysis.

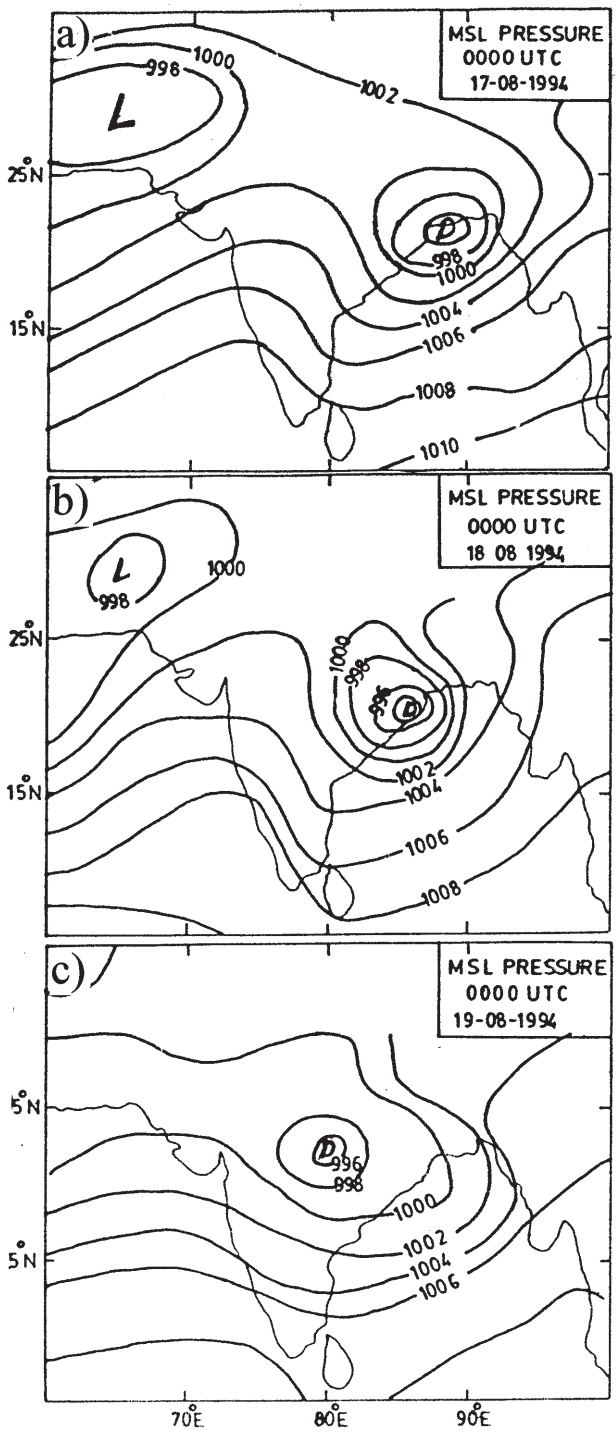

Figure 3. *Observed mean sea level pressure (contour interval: 2 hPa) at 0000 UTC on (a) 17 August 1994, (b) 18 August 1994 and (c) 19 August 1994. (Source: India Met. Dept.)*

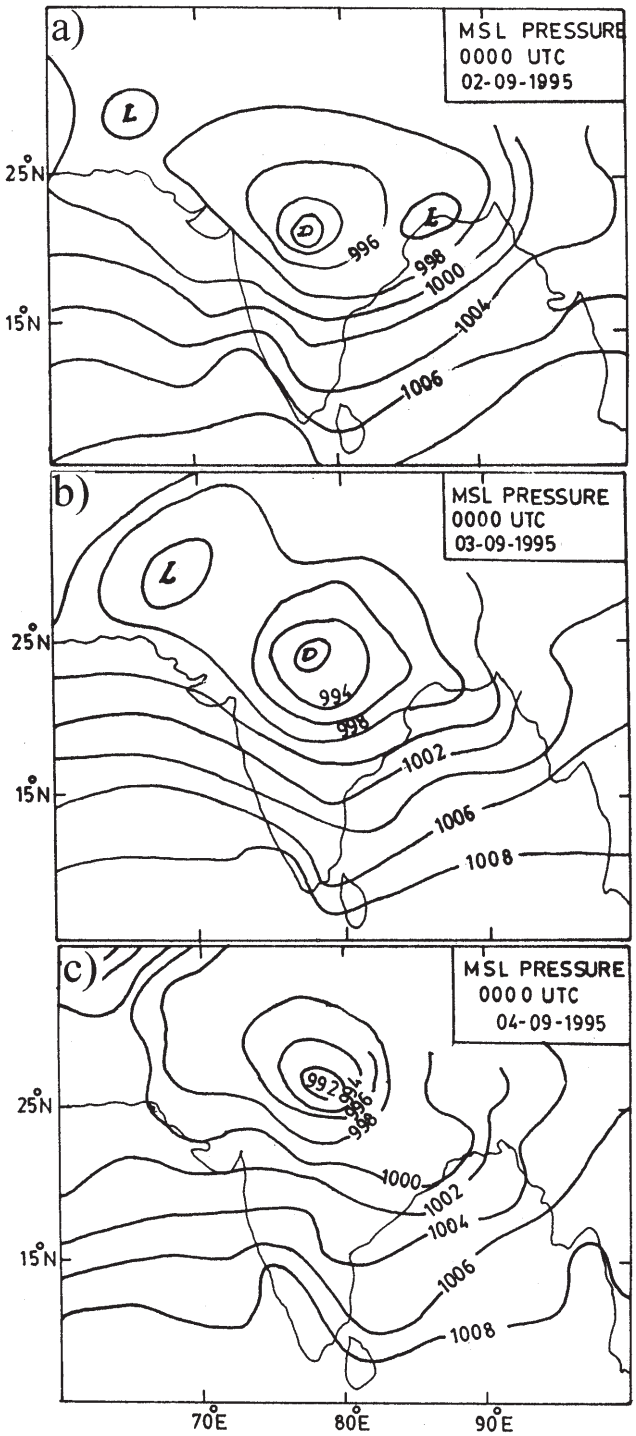

Figure 4. *Observed mean sea level pressure (contour interval: 2 hPa) at 0000 UTC on (a) 2 September 1995, (b) 3 September 1995 and (c) 4 September 1995. (Source: India Met. Dept.)*

For Case II, the 24-hour forecast of mean sea level pressure (Figure 5(*d*)) is comparable with that analysed (Figure 5(*c*)). However, the predicted central pressure is about 2 hPa higher than the actual value near the depression, and in other regions this difference has increased to 4 hPa. The analysed mean sea level pressure at the centre of the depression was 995.4 hPa and that simulated by the model was 997.1 hPa. The location of the model-predicted centre is very close to that of the analysis field.

The forecast mean sea level pressure at 0000 UTC on 18 August 1994 for Case III shows that the model could simulate the depression centre well, though the pressure is over-estimated by 2 hPa at the centre of the storm. The centre of the depression predicted by the model is close to that observed.

The mean sea level pressure forecast and verifying analysis for Case IV (Figure 5(*g*)) also show that the depression has been simulated well by the model

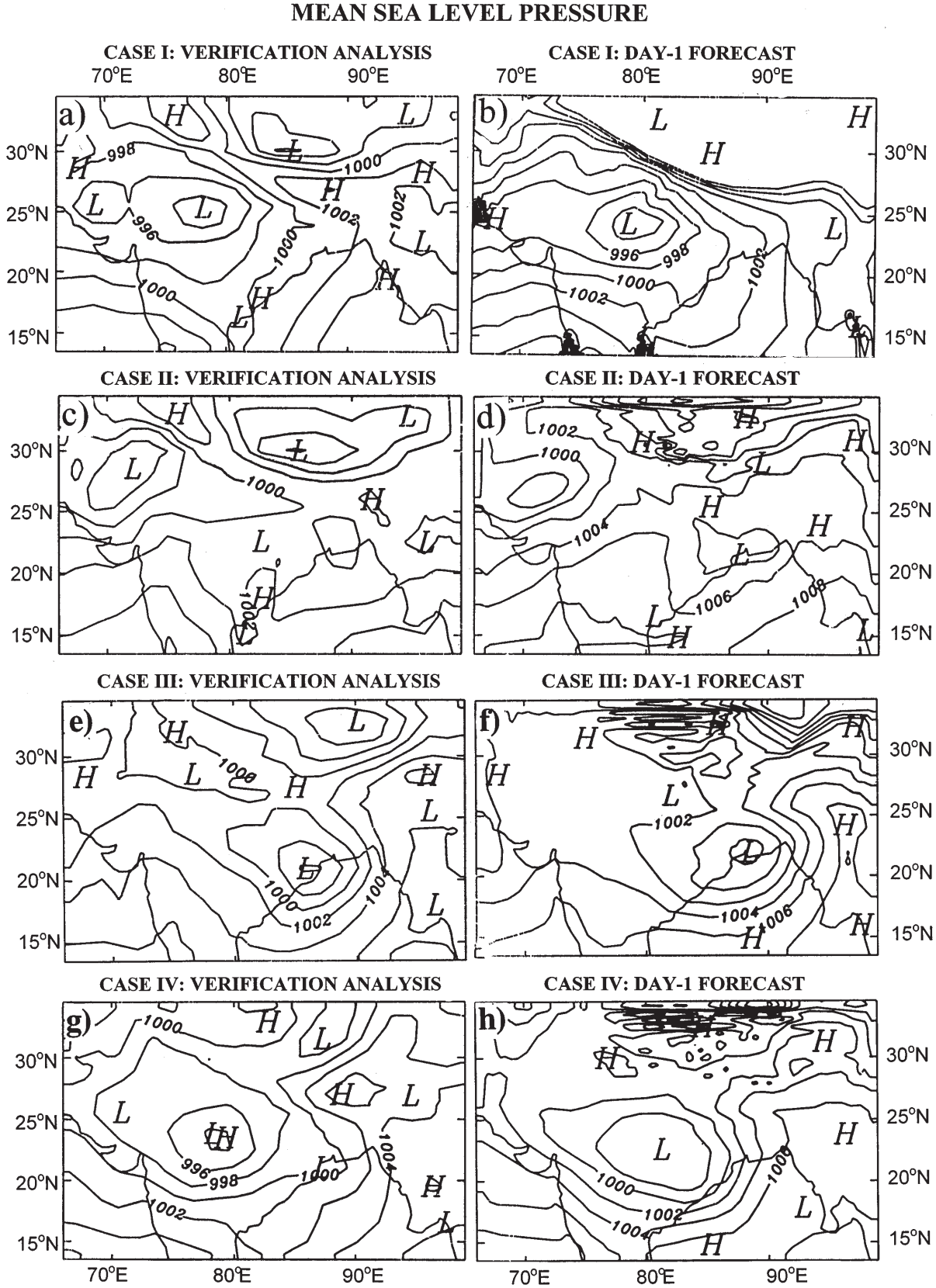

Figure 5. *(a) Verification analysis of mean sea level pressure for 1200 UTC on 4 August 1988 (Case I) and (b) the corresponding 24-hour forecast. (c), (d) As for (a), (b) but for 1200 UTC on 6 August 1988 (Case II). (e), (f) As for (a), (b) but for 0000 UTC on 18 August 1994 (Case III). (g), (h) As (a), (b) but for 0000 UTC on 3 September 1995 (Case IV).*

Table 2. *Comparison of model forecast and corresponding verification analyses of the central pressure of the monsoon depressions and their location.*

Cases	Time of model integration	Verification analysis		Model forecast	
		Central pressure (hPa)	Location of the central pressure	Central pressure (hPa)	Location of the central pressure
Case I	24 hour	993.2	24.0 °N, 79.0 °E	993.6	25.5 °N, 78.5 °E
	48 hour	993.5	27.0 °N, 72.5 °E	996.2	22.5 °N, 81.0 °E
Case II	24 hour	995.4	27.5 °N, 70.5 °E	997.1	26.0 °N, 70.5 °E
	48 hour	993.6	30.5 °N, 72.5 °E	1001.5	27.5 °N, 72.5 °E
Case III	24 hour	996.0	21.0 °N, 86.0 °E	996.4	21.5 °N, 87.0 °E
	48 hour	995.9	22.5 °N, 80.0 °E	1001.3	22.5 °N, 81.0 °E
Case IV	24 hour	993.4	23.5 °N, 78.5 °E	996.3	22.5 °N, 80.0 °E
	48 hour	995.7	28.0 °N, 75.0 °E	999.1	25.0 °N, 75.5 °E

(Figure 5(*h*)). The location of the centre of the depression agrees reasonably well with the verification analysis. The analysis at 0000 UTC on 3 September 1995 shows a pressure minimum of 993.4 hPa at the centre of the depression, whereas that simulated by the model is 996.3 hPa. Owing to the extrapolation of the surface pressure forecast field to mean sea level, sometimes certain distortions are observed in pressure contours over the Himalayan region. Satisfactory performance of the model has been seen in the 48-hour forecast as well, although we have not provided any figures to show this.

5. Wind forecasts

Figure 6 depicts the 24-hour forecast of wind vector and isotachs at the 0.9 σ level for all four cases, along with the verification analysis fields. In each case, the wind flow around the depressions has been simulated satisfactorily by the model. This feature is also very clear in the streamline forecasts (not shown). In general, the model over-predicts wind speed over the eastern and southern sectors of the depression. The main forecast error seems to be over the Himalayan region owing to the high orography. One of the observed features of monsoon depressions is the presence of strong winds over the northern quadrant (Rao, 1976). This feature can be seen in the analyses for each case and the corresponding wind forecasts.

The maximum wind speed simulated by the model for Case I was 16.1 m s^{-1} on the northern side of the vortex, and the corresponding observed wind speed was 14.8 m s^{-1}. Over the oceanic regions, as well as over the peninsular Indian region, the model was able to accurately predict the wind. However, as indicated above, over the Himalayan region, simulated wind fields are found to be higher than those observed.

For Case II, the location of the depression is close to that observed. But the magnitude of winds simulated by the model around the depression is higher than that analysed: the model predicted wind up to 12 m s^{-1}, though the actual wind was less than 10 m s^{-1}. Higher winds were predicted over the Arabian Sea and Bay of Bengal. This could be due to the coarser resolution of the initial conditions used compared with the model resolution (50 km).

There is a reasonably good prediction of the depression centre in Case III. However, over the northern quadrant of the depression, higher winds were predicted (21.2 m s^{-1}) compared with those observed (16.3 m s^{-1}). Higher winds (up to 21.8 m s^{-1}) are also predicted over the Himalayan region.

For Case IV, the cyclonic circulation and strong westerly wind at the southern part of the depression are well predicted by the model. However, the magnitude of the wind predicted by the model towards the northern quadrant of the depression was about 7 m s^{-1} higher than in the analysis field and about 6 m s^{-1} higher over the peninsular region. The maximum wind speeds given by the verification analysis at the northern and the southern parts of the depression are 18.4 m s^{-1} and 21 m s^{-1} respectively, and the corresponding values predicted by the model are 25.4 m s^{-1} and 25.3 m s^{-1}. The model predicted higher winds over the Himalayan region as well.

6. Temperature forecasts

Figure 7 illustrates the 24-hour forecast of air temperature at the 0.9 σ level for all four cases, along with the corresponding verification analysis. In the analysis for Case I, the peninsular Indian region had an air temperature of about 296 K at 1200 UTC on 4 August 1988, and the forecast had about the same value. For Case II, the 24-hour air temperature at the 0.9 σ level is reasonably good, though it over-estimated the value along the east coast of India and peninsular region by about 2 K. The whole of peninsular India except the southern tip

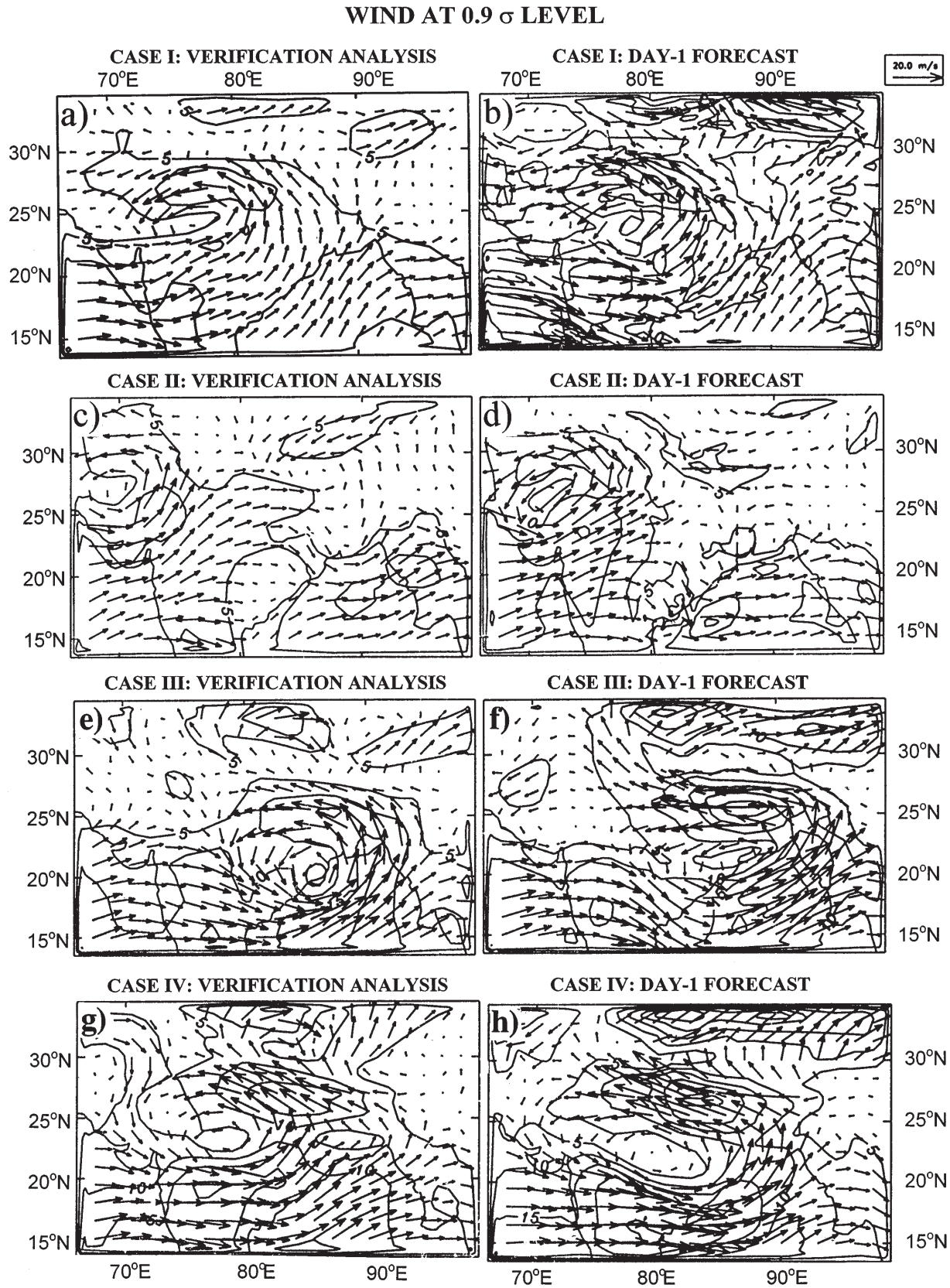

Figure 6. *As Figure 5 but for wind at the 0.9 level.*

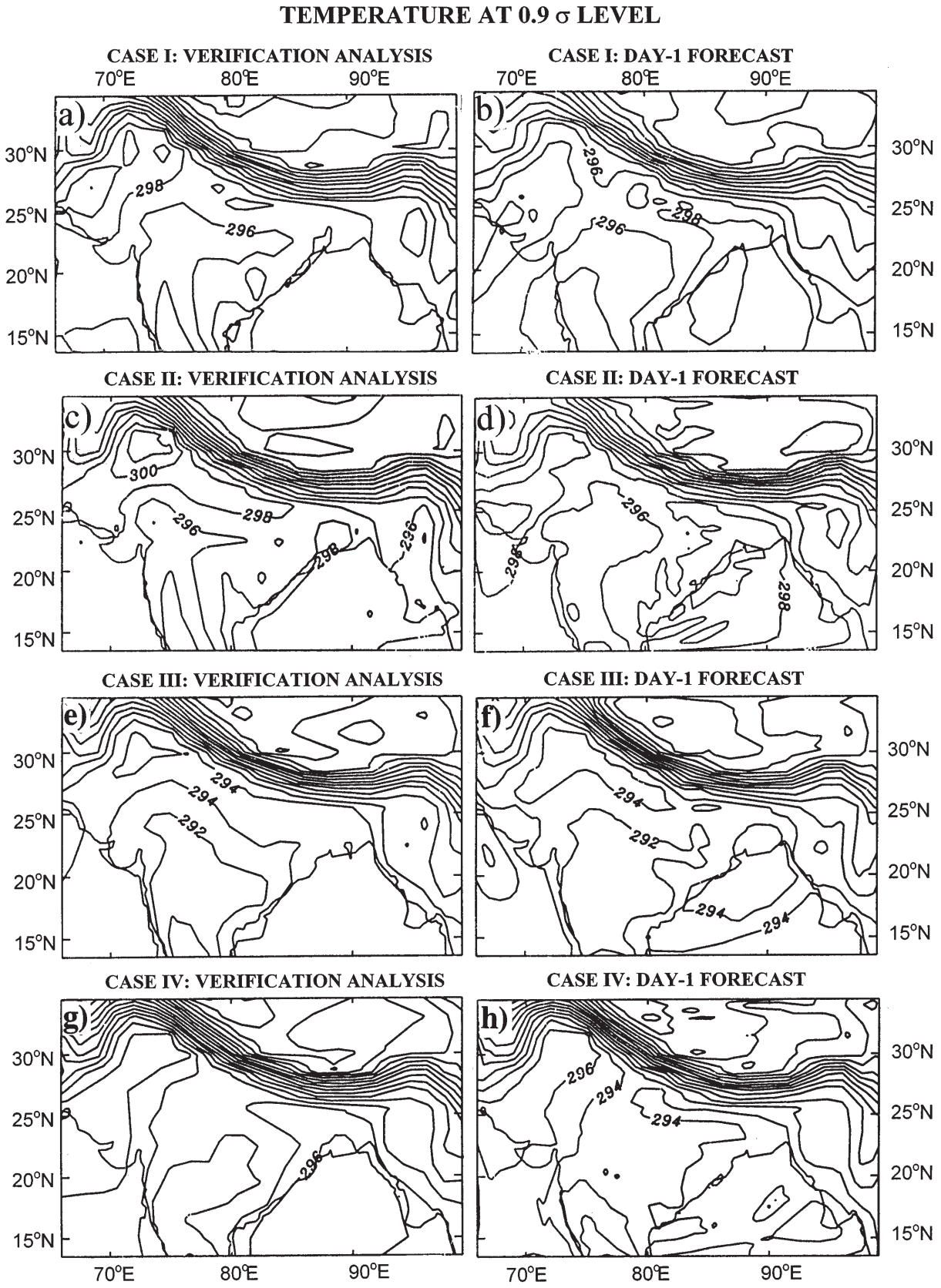

Figure 7. *As Figure 5 but for temperature at the 0.9 level.*

has a temperature of 292 K in both the forecast and the analysis fields. Although a closed isotherm of 294 K can be seen in the verification field over the Head Bay of Bengal at about 22° N, 90° E, it covers a wider area in the forecast field. Over the western part of the domain, an increase of 2 K is seen in the verification field. A reasonably good forecast of air temperature can be seen for Case III as well. The whole peninsular region was covered by a 293 K isotherm at the 0.9 σ level by the model forecast and the verification analysis. Around the depression centre, the verification analysis shows a 294 K closed isotherm, but this isotherm was spread over a wider region in the model forecast. Thus, the model provides a good simulation of temperature at lower levels with a difference in temperature of about 1–2 K between the forecast and the corresponding verification analysis. Similar behaviour can be seen in each case at higher levels and for the 48-hour forecast (not shown). In general, the model is able to simulate the temperature field reasonably well.

7. Rainfall forecasts

Isohytes of observed rainfall for the period 0300 UTC, 4 August 1988 to 0300 UTC, 5 August 1988 (accumulated rainfall for a 24-hour period) are given in Figure 8(*a*). Since daily observations of rainfall are available at 0300 UTC, the rainfall forecast between 15 and 39 hours of model integration (i.e., 0300 UTC, 4 August 1988 to 0300 UTC, 5 August 1988) has been accumulated and presented here for the whole domain of FRG. Over the depression zone, the model produced a fair amount of precipitation (10.1 cm) over a wide region. Over the east coast of India, the rainfall produced by the model is comparable with the observed values.

The precipitation forecast for Case II between the 15 and 39 hours of model integration (accumulated 24-hour rainfall) is given in Figure 8(*d*), and the corresponding observed 24-hour rainfall ending at 0300 UTC on 7 August is given in Figure 8(*c*). The model forecast 5.8 cm of rain towards the south-west quadrant of the depression during the period as against the observation of 11 cm at a nearby station. Towards the east coast of India, 6 cm rainfall was recorded. The model predicted 9.3 cm at the grid point close to that station.

Figure 8(*f*) illustrates the total predicted rainfall accumulated over a 24-hour period for Case III. This accumulation is carried out between 3 and 27 hours of the model integration as the model had initial conditions from 0000 UTC. The observed accumulated rainfall for 24 hours ending at 0300 UTC on 18 August 1994 is presented in Figure 8(*e*). Beyond 90° E, the model predicted heavy rainfall; however, there are no observations over the region. Towards the southern quadrant of the depression, at 85.5° N, rainfall of 6.8 cm is predicted. During the period, Bhubaneswar (20.0° N, 85.5° E) received a rainfall of 16 cm. Along the west coast, a nearby station recorded 10 cm of rainfall, but the model could simulate less than 1 cm rainfall over the region. Higher rainfall has been reported at about 16° N and 78° E. Hyderabad (17.2° N, 78.3° E) reported a rainfall of 7 cm during the period, with the model producing only 2.6 cm of rainfall over the same region. Forecast of total precipitation of the model is the sum of cumulus convection and large-scale precipitation. Initial conditions for the moisture as well as horizontal convergence of the moisture may have caused under-estimation of rainfall prediction. Limitations of the cumulus parameterization scheme used in the model might also have contributed for these under-predictions.

For Case IV, 24-hour accumulated precipitation between 3 and 27 hours of model integration is given in Figure 8(*h*). The corresponding observed accumulated rainfall ending at 0300 UTC on 3 September 1995 is presented in Figure 8(*g*). The forecast field shows good agreement with that observed over the south-western quadrant of the depression zone. The maximum precipitation simulated over the zone is 6.1 cm as against the observation of 8 cm. Over the west coast, precipitation of 2.5 cm is predicted with the model compared to 4 cm recorded rainfall during the same period.

8. Vertical cross-sections

Forecasts and the corresponding analysis fields of wind and temperature are averaged along the meridional direction, and their vertical-cross-sections are analysed to study the monsoon depression characteristics. Since for all the cases the characteristics are similar, only those for Case I are presented here. For averaging, the latitudes from 22° to 27° N have been chosen so that it covers almost the entire monsoon trough region and the depression track.

The north–south averaged vertical cross-sections of the zonal component of the wind (for Case I) are presented in Figure 9. Figure 9(*a*) depicts the meridional cross-section of the verification analysis for 4 August 1988 at 1200 UTC, and Figure 9(*b*) illustrates the vertical cross-section of the corresponding 24-hour forecast. The analysis shows that the prevailing wind up to 78° E is easterly, and beyond that longitude it is westerly. A part of the Head Bay of Bengal region also has come under the averaging zone. The westerly wind beyond 78° E is attributed to the influence of strong westerly wind over the Head Bay of Bengal. The model simulated the same structure of westerly wind beyond 78° E, though the wind magnitude is higher than the verification analysis. Up to 78° E, the verification analysis shows easterly winds up to the 0.85 σ level (Figure 9(*a*)). The model could simulate the same feature of easterly wind up to 78° E, though a zone of westerly wind is simulated at the lower levels at about 73° E.

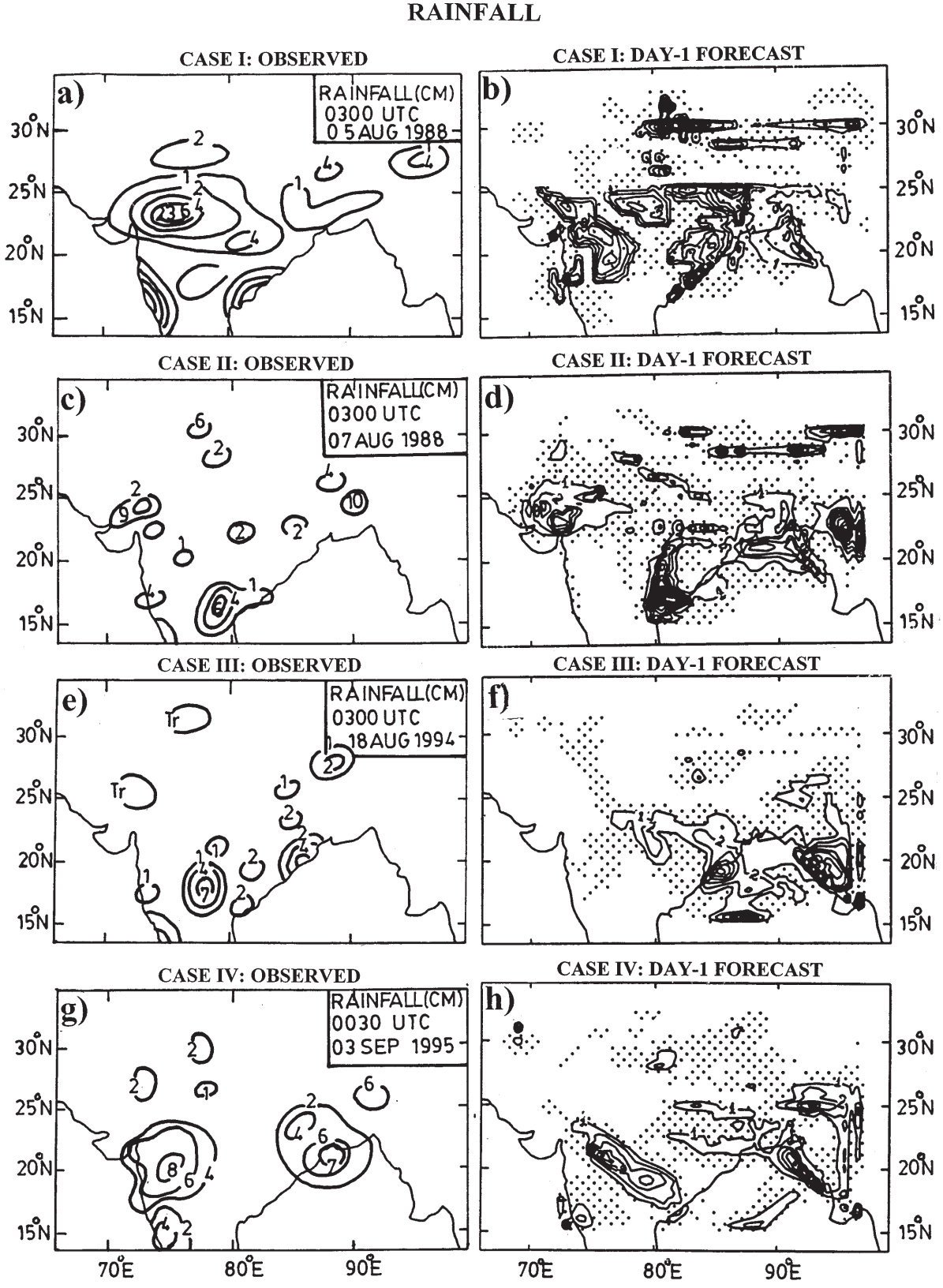

Figure 8. *As Figure 5 but for precipitation.*

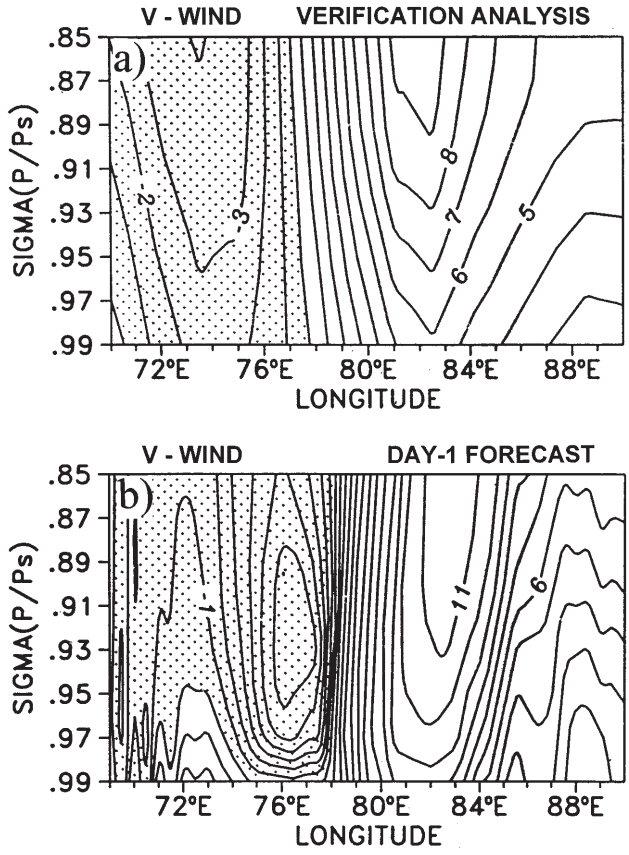

Figure 9. *Meridionally averaged zonal component of wind with height (unit: m s^{-1}) for the Case I for (a) verification analysis and (b) 24-hour forecast. Shaded area shows easterly winds.*

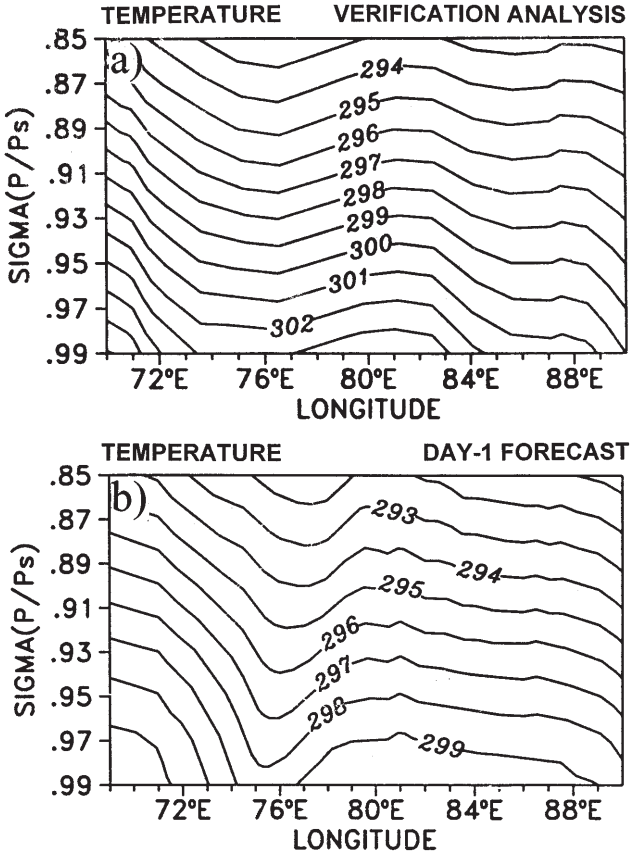

Figure 10. *As Figure 9 but for temperature (unit: K).*

The vertical cross-section of meridionally averaged air temperature of the verification analysis for 4 August 1988 at 1200 UTC and the corresponding 24-hour forecast from the model are presented in Figure 10. It is observed that a monsoon trough has a warm west side (Rao, 1976), and this feature is simulated by the model. Similarly the relatively warm northern side of the monsoon trough has been well simulated. Another important feature of the monsoon depression is its cold core structure (Rao, 1976). This specific feature is also simulated well by the model. Observational studies show that monsoon depressions generally slope in a southwest direction with height. Though Figure 10(*b*) shows an eastward tilt very close to the surface, its slope reduces with height. Since the analysis is being done for very coarse vertical resolutions (1000 and 850 hPa), these features are not found in the verification analysis. However, the model has a much higher vertical resolution in the lower troposphere (eight levels in the PBL), and hence these features could be simulated well.

9. Root mean square error of forecasts

To examine the performance of the model in a quantitative manner, the root mean square (RMS) errors are computed at different levels (σ = 0.25, 0.55 and 0.9) for winds (u and v components), temperature and surface pressure for all cases. Table 3 shows the RMS error for both 24- and 48-hour forecasts. The tabulated values clearly show that, in general, the large-scale fields are well simulated by the model in each case. For most fields, the RMS error is less at 24 hours rather than 48 hours. Another important aspect is that the RMS error difference between the 24- and 48-hour forecasts decreases with height. Surface and boundary layer processes are very important in simulating the monsoon depressions because they are confined to the lower troposphere. Large RMS errors at lower levels show that the parameterization for boundary layer and surface processes in the present version of the model do not fully represent the physical processes.

10. Track predictions

For all cases the 48-hour forecasts of the tracks of the monsoon depressions are illustrated in Figure 11 along with the analysed tracks. This figure shows that the model simulated the track reasonably well, but in all cases the observed tracks do not exactly match with those analysed. If we examine the forecast track, it is interesting to note that in three out of the four cases, the observed track is closer to the forecast track than the analysed track. The simulated speed of the depression is also less than that analysed.

Table 3. *RMS error of temperature and wind (both meridional and zonal component) at different levels and mean seal level pressure computed by the model for all cases.*

Case	Surface pressure (hPa)		Level (σ)	u (ms^{-1})		v (ms^{-1})		Temperature (K)	
	24 hour	48 hour		24 hour	48 hour	24 hour	48 hour	24 hour	48 hour
Case I	2.72	3.94	0.25	8.13	8.40	8.36	8.10	1.81	2.56
			0.55	3.51	5.53	2.57	4.31	1.08	1.05
			0.90	4.81	7.29	2.84	7.61	1.74	2.97
Case II	3.21	5.92	0.25	7.22	6.88	7.08	7.37	1.91	2.67
			0.55	3.10	4.87	2.59	3.95	0.92	1.22
			0.90	3.00	3.81	2.63	3.07	1.64	2.13
Case III	0.44	4.96	0.25	6.90	6.34	6.96	6.67	1.74	2.07
			0.55	2.89	4.62	2.64	2.88	1.46	1.35
			0.90	4.61	4.53	2.98	2.39	1.26	1.47
Case IV	2.51	3.87	0.25	7.72	7.11	7.21	5.53	1.42	1.49
			0.55	4.60	3.45	4.49	3.08	1.39	1.29
			0.90	5.46	5.38	4.06	3.85	1.06	1.38

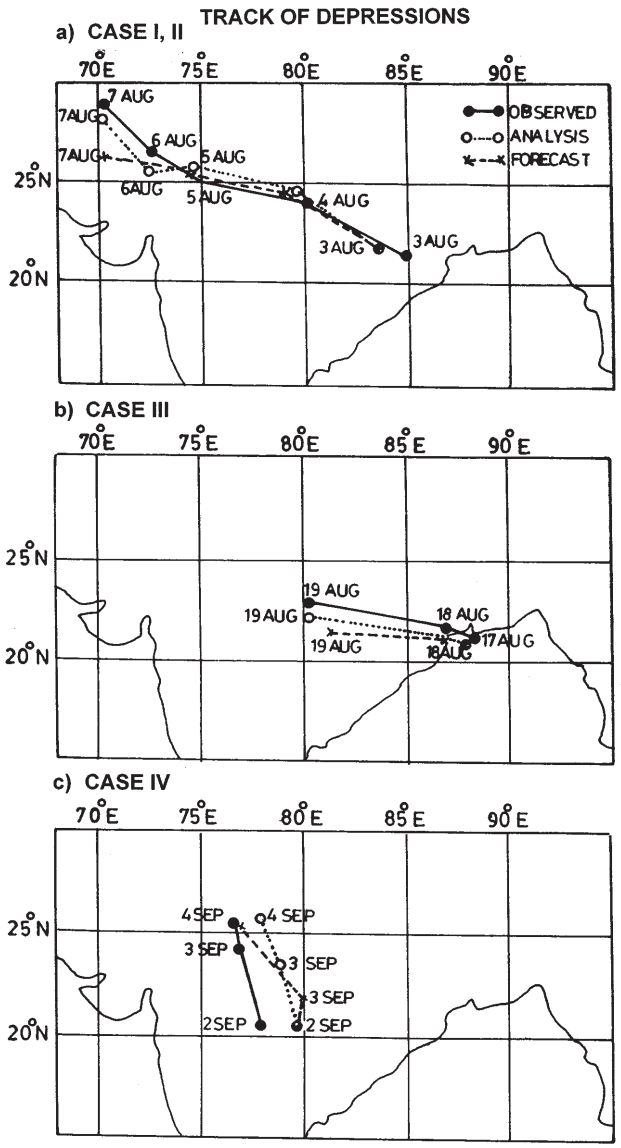

Figure 11. *Trajectory of the depressions obtained from the model forecast, observations and analysis for (a) 3–7 August 1988, (b) 17–19 August 1994 and (c) 2–4 September 1995.*

To study the error of the forecast track in detail, both positional and directional errors of the tracks are presented in Table 4. For this purpose, both the 24- and 48-hour forecasts have been taken into consideration.

- The positional error is taken to be the distance between the centre of the forecast depression and that of the corresponding verification analysis.
- The directional error is computed as the angle between the straight lines connecting the initial model analysis and the forecast and the corresponding verification analysis.

Let x_0 and y_0 be the longitude and latitude coordinates of the initial position of the centre of the depression. Similarly, let x_F and y_F represent the centre coordinates after a 24-hour forecast and x_V and x_V represent the coordinates of the depression for the corresponding verification analysis. The directional error is computed as:

$$\left(\frac{y_V - y_0}{x_V - x_0}\right) - \tan^{-1}\left(\frac{y_F - y_0}{x_F - x_0}\right)$$

The results show that the positional error is smaller for the 24-hour forecast than that for the 48-hour forecast, suggesting that, with the increase of model integration period, the centre of the depression moves away from the corresponding analysis. However, the directional error for each case shows that with the increase in time of model integration, the simulated depression centre converges towards the corresponding verification analysis. In each case, the directional error is less for the 48-hour forecast than for the 24-hour one. From Figure 11, it can be seen that, in general, the speed of the simulated depression is less than that of the analysed and observed ones. Hence the positional error increases with increase of model integration period.

Table 4. *Distance and directional errors of the track of the four depressions for both 24-hour and 48-hour forecasts.*

Error	Case I		Case II		Case III		Case IV	
	24 hour	48 hour	24 hour	48 hour	24 hour	48 hour	24 hour	48 hour
Positional error (km)	173.9	352	165	330	110	123.2	206.2	334.8
Directional error (degrees)	11.3	0.30	15.25	0.22	26.56	1.5	36.8	14.5

11. Conclusions

The following conclusions are drawn from the simulation of four distinct monsoon depressions using the fine-resolution grid of a regional double-nested model.

- In all cases, the model could simulate the large-scale fields such as mean sea level pressure, wind and temperature reasonably well up to 48 hours of integration. Even for the 48-hour forecast, the location of the centre of the depression matches well with that of the verification analysis, though the magnitude of the central pressure is higher than that analysed.
- The precipitation field predicted by the model for all cases can be compared with the observations. The distribution of precipitation in and around the depression zone in the model in each case is slightly under-predicted. Observed maximum precipitation over the south-west quadrant of the depression has also been simulated by the model for each case.
- The vertical cross-section of temperature shows that the cold core structure of monsoon depressions has been predicted by the inner fine-resolution grid (FRG) model. This shows the importance of horizontal resolution for the simulation of monsoon depressions apart from the importance of vertical resolution and orography.
- Computed RMS errors for the large-scale fields show that the model, in general, is able to simulate monsoon depressions well. The RMS error decreases with height, which indicates the importance of surface processes in simulating the monsoon depressions and the lack of adequate representation of physical processes in the present version of the model.
- Predictions of monsoon depression tracks show that with the increase of model integration time, the depression centre converges towards the analysis, though the predicted speed of the depression is less compared with the observations and the model analysis.

Acknowledgments

The authors would like to acknowledge the computer resources provided by the National Centre for Medium Range Weather Forecasting, New Delhi, India. Part of the work was supported by the Office of Naval Research, USA and Department of Science and Technology, New Delhi, India.

Appendix. Model details

A primitive-equation nested-grid model with terrain-following coordinate (σ coordinate system) is used in this study. The finite difference form of the governing equations used in the model is of second-order accuracy in space. The time integration scheme is split-explicit (Madala, 1978), which allows a larger time step by effectively separating various terms in the prognostic equations into parts governing slow-moving Rossby modes and fast-moving gravity modes. Details of the time integration scheme employed in the model have been given by Mohanty *et al.* (1990). For horizontal differencing, a staggered Arakawa C-grid (Arakawa & Lamb, 1977) is used with a uniform resolution in longitude and latitude. In this grid system, temperature (T), geopotential (ϕ), humidity (q) and σ are computed at mass points. The zonal component of the wind (u) is computed at the mid-points of mass points along the x axis and the meridional component (v) is computed at mid-points along the y axis, and the vertical velocity ($\dot{\sigma}$) is evaluated at half σ levels. The sponge boundary condition of Perkey & Kreitzberg (1976) is employed for updating the lateral boundaries of the model, and a second-order diffusion equation is used in the model to suppress the computational instabilities, which arise owing to unresolved sub-grid scale processes. More details about the model equations and numerics may be obtained from Madala *et al.* (1987).

The model has a fine resolution grid (FRG) part and a coarse-resolution grid (CRG) part. Details about these two parts are given in Table A1.

The FRG part has been embedded in the CRG. Both the parts have 16 levels in the vertical with 8 levels in the PBL. The model has been nested in such a way that the flow of information is only from CRG to FRG and every third point of the FRG is collocated with the CRG grid points. The nested grid is also positioned in such a way that its boundary rows and columns overlap the CRG interior rows and columns. This nesting configuration enables the FRG domain boundary values to be specified by the CRG interior grid points. Lateral boundary conditions are provided in the models

Table A1. *An overview of the nested grid model.*

Description	Fine-resolution grid model	Coarse-resolution grid model
Domain	66°–99° E, 13.5°–34.5° N	30°–120° E, 15° S – 45° N
Independent variables	λ, Φ, σ, t	
Prognostic variables	u, v, T, q, p_s	
Diagnostic variables	φ, σ	
Topography	Envelope (mean + 1 standard deviation)	
Vertical grid system	16 levels in σ coordinates	
Vertical levels	0.05, 0.15, 0.25, 0.35, 0.45, 0.55, 0.65, 0.75, 0.82, 0.86, 0.9, 0.935, 0.96, 0.975, 0.987, 0.997	
Horizontal grid	Arakawa C grid	
Integration scheme	Split-explicit time integration	
Time step	150 seconds	450 seconds
Horizontal grid lengths (,)	1.5° latitude/longitude	0.5° latitude/longitude
Horizontal diffusion	Linear second order	
Initialization	Non-linear normal mode	
Physical processes	Dry convective adjustment; cumulus convection (Anthes, 1977); large-scale precipitation with RH > 95%; PBL: Monin–Obukhov similarity theory for the surface layer coupled with TKE closure scheme for the PBL	

based on the scheme of Davies (1976, 1983). Therefore, for any dependent variable a:

$$a = (1 - \alpha)a_m + \alpha\, a_b$$

where the subscript 'm' represents the FRG model computed value and the subscript 'b' represents the boundary value obtained either from observations or from the CRG model. The merging is done for the outer six points at the boundaries of both the model part domains; α is defined as a quadratic function of the minimum distance from the lateral boundary in units of the grid spacing (Gronas *et al.*, 1987). At each time step, the boundary values a_b for the CRG are obtained through a linear interpolation in time from the analysed data set. For the FRG domain, lateral boundary conditions a_b are obtained through a linear interpolation in time and space from the CRG domain.

The physical processes included in the model are associated with dry convective adjustment, large-scale precipitation, convective precipitation and the planetary boundary layer (PBL). Deep cumulus convection is parameterized on the basis of the scheme of Kuo (Anthes, 1977). Convective precipitation occurs when low-level moisture convergence exists in a convectively unstable environment. The partitioning of the latent heating and moisture is determined by the column mean relative humidity. The vertical distribution of the heating is considered to be proportional to the temperature difference between the pseudo-adiabat and the environment. Large-scale precipitation (non-convective) occurs when saturation is reached on the grid scale. The Clausius–Clapeyron equation is used to compute the excess moisture and the isobaric heating; depending on the height where the saturation occurs, a point of the excess moisture is assumed to precipitate into lower model layers and to re-evaporate. The remainder of the excess moisture precipitates to the surface. Dry convective adjustment is used when the static energy of the layer exceeds that of the adjacent higher layer. The adjustment results in slightly stable lapse rate, while the total static energy is conserved. Potty *et al.* (1997) studied the effect of different boundary layer parameterization schemes using first-order and one-and-a-half-order closure schemes for the simulation of the monsoon depression using a high-resolution regional model. They found that Monin–Obukhov similarity theory for the surface layer coupled with a turbulent kinetic energy (TKE) closure scheme for the upper layers performed reasonably better. Hence for the present study, boundary layer processes are parameterized by using Monin–Obukhov similarly theory (Businger *et al.*, 1971) for the surface layer and the TKE closure scheme with the constants of Detering & Etling (1985) for the PBL. The time steps for the slow-moving modes in CRG and FRG are 450 and 150 seconds respectively. Model grid topography for both the model domains is obtained from the US Navy 10′ × 10′ global topography data set.

References

Anthes, R. A. (1977). A cumulus parameterization scheme utilizing a one-dimensional cloud model. *Mon. Wea. Rev.*, **105:** 270–286.

Arakawa, A. & Lamb, V. R. (1977). Computational design of the basic dynamical process of the UCLA general circulation model. In: *Methods in Computational Physics* (edited by J. Chang). Academic Press. **17**, 173–265.

Asnani, G. C. (1993). Tropical Meteorology. Published by Prof. G. C. Asnani. 1202 pp.

Businger, J. A., Wyngaard, J. C., Izumi, Y. & Bradley, E. F. (1971). Flux profile relationship in the atmospheric surface layer. *J. Atmos. Sci.*, **28:** 181–189.

Das, P. K. (1952). Monsoon depressions in the Bay of Bengal. *Indian J. Meteorol. Geophys*., **3:** 225–229.

Davies, H. C. (1976). A lateral boundary formulation for multi-level prediction models. *Q. J. R. Meteorol. Soc.,* **102:** 405–418.

Davies, H. C. (1983). Limitations of some common lateral boundary schemes used in regional NWP models. *Mon. Wea. Rev.,* **111:** 1002–1012.

Detering, H. W. & Etling, D. (1985). Application of the $E - \varepsilon$ turbulence model to the atmospheric boundary layer. *Boundary-Layer Meteorol*., **33:** 113–133.

Godbole, R. V. (1977). The composite structure of the monsoon depression. *Tellus*, **29:** 25–40.

Gronas, S., Foss, A. & Lystad, M. (1987). Numerical simulations of polar lows in the Norwegian Sea. *Tellus*, **39A:** 334–353.

Koteswaram, P. & George, C. A. (1958). On the formation of monsoon depressions in the Bay of Bengal. *Indian J. Meteorol. Geophys.,* **9:** 9–22.

Krishnamurti, T. N. (1977). Primitive equation models and their application to the tropics. In: *WMO Report No. 492*, World Meteorological Organization, Geneva, Switzerland, pp. 193–214.

Krishnamurti, T. N., Kanamitsu, M., Godbole, R., Chang, C. B., Carr, F. & Chow, J. H. (1976). Study of a monsoon depression. II. Dynamical structure. *J. Meteorol. Soc. Japan,* **54:** 208–225.

Krishnamurti, T. N., Molinari, J., Pan, H. L. & Wong, V. (1977). Downstream amplification and formation of monsoon disturbances. *Mon. Wea. Rev.,* **105:** 1281–1297.

Krishnamurti, T. N., Low-Nan, S. & Pash, R. (1983). Cumulus parameterisation and rainfall rates. II. *Mon. Wea. Rev.*, **111:** 815–828.

Krishnamurti, T. N., Ingles, K., Cocke, S., Pasch, R. & Oodally, W. (1984). Details of low latitude medium range numerical weather prediction using a global spectral model. II. *J. Meteorol. Soc. Japan,* **62:** 613–649.

Lindzen, R. S., Farrell, S. & Rosenthal, A. J. (1983). Absolute barotropic instability and monsoon depressions. *J. Atmos. Sci.,* **40:** 1178–1184.

Madala, R. V. (1978). Efficient time integration schemes for atmosphere and ocean. Finite difference techniques for vectorized fluid dynamics calculations. Springer-Verlag, pp. 56–74.

Madala, R. V., Chang, S. W., Mohanty, U. C., Madan, S. C., Paliwal, R. K., Sarin, V. B., Holt, T. & Raman, S. (1987). Description of Naval Research Laboratory limited area dynamical weather prediction model. *NRL Tech. Report 5992, Washington DC*, 131 pp.

Mohanty, U. C., Paliwal, R. K. & Tyagi, A. (1990). Application of split-explicit time integration scheme to a multi-level limited area model and forecast performance over the Indian region. *Mausam*, **41:** 531–540.

Mooley, D. A. & Shukla, J. (1987). Variability and forecasting of the summer monsoon rainfall over India. In: *Monsoon Meteorology* (edited by C. P. Chang & T. N. Krishnamurti). Oxford University Press, New York, 544 pp.

Pearce, R. P. (1981). Downstream development of baroclinic waves in the upper-tropospheric monsoon easterlies suggested by a simple model experiment. In: *Monsoon dynamics* (edited by J. Lighthill & R. Pearce). Cambridge University Press, pp. 381–402.

Perkey, D. J. & Kreitzberg, W. (1976). A time dependent lateral boundary scheme for limited area primitive equation models. *Mon. Wea. Rev.,* **104:** 744–755.

Pisharoty, P. R. & Asnani, G. C. (1957). Rainfall around monsoon depressions over India. *Indian J. Meteorol. Geophys.* **8:** 15–20.

Potty, K. V. J., Mohanty, U. C. & Raman, S. (1997). Effect of three different boundary layer parameterisations in a regional atmospheric model for the simulation of summer monsoon circulation. *Boundary Layer Meteorol.*, **84:** 363–381.

Rao, K. V. & Rajamani, S. (1970). Diagnostic study of a monsoon depression by the geostrophic baroclinic model. *Indian. J. Meteorol. Geophys.*, **21:** 187–194.

Rao, Y. P. (1976). Southwest monsoon. *Meteorological Monograph*, *Synoptic Meteorology*, No. 1/1976, India Meteorological Department, India, 367 pp.

Shukla, J. (1977). Barotropic–baroclinic instability of mean zonal wind during summer monsoon. *Pure Appl. Geophys.,* **115:** 1449–1461.

Sikka, D. R. (1977). Some aspects of the life history, structure and movement of monsoon depressions. *Pure Appl. Geophys.,* **115:** 1501–1529.

Srinivasan, V., Raman, S. & Ramakrishnan, A. R. (1971). Monsoon depression as seen in satellite pictures. *Indian J. Meteorol. Geophys.*, **21:** 187–194.

Warner, C. (1984). Core structure of a Bay of Bengal monsoon depression. *Mon. Wea. Rev.,* **112:** 137–152.